

# 3D Segmentation and Volumetric of Growth Plate of Radius Bone for Legal Age Determination in MRI Data Set

Hamed Yousefi<sup>1</sup>      Mansoor Fatehi<sup>2</sup>      Reza Aghaeizadeh Zoroofi<sup>1</sup>

<sup>1</sup>School of Electrical and Computer Engineering, College of Engineering, University of Tehran, Iran  
<sup>2</sup>Director, Medical Imaging Informatics Research Center

**Abstract**—The most prominent difference between an immature skeleton and a mature adult skeletal system is the presence of a Physis which is also known as the growth plate. In this paper a methodological approach based on 3D level set is proposed for fully automated segmentation of Growth plate in Radius bone. The implemented algorithm consists of several stages for a successful segmentation. In the first step, Radius bone is extracted using 3D active contour method. After extracting the Radius bone, to obtain the growth plates the ROI should be extracted according to anatomical information and bone shape. The main challenge in segmenting the growth plates occurs when these plates get closed and narrowed due to aging. For enhancing the contrast in this step, a Gabor filter is used, and finally using sphere spaces as the primary mask of level-set algorithm, a 3D segmentation of Radius Growth plate can be performed. We utilize the proposed approach as part of a computer-aided diagnosis system for robust legal age determination.

**Keywords** — Growth plate, Bone age determination, 3D level set, Segmentation, Gabor filter

## I. INTRODUCTION

A challenge that FIFA's medical team concern about is the difference between players' real ages and the age printed on the identity document. Football players are categorized into different age orders according to their ages. In many Asian and African countries there is no access to a reliable system to determine the actual birth date, and this date can be manipulated easily [1][2]. This issue results in several complaints each year. According to physiological studies, bone age has the highest correlation with chronological age. There are cartilage like Growth plates in wrist hand bones which ossify as people get older. One of these growth plates is located in Radius bone. The ossification of this plate is the principal criterion for legal age determination [3]. Accordingly, Through MR imaging of hand wrist, we can analyze this growth plate [4]. According to the thickness and light intensity of the Radius bone's growth plates, FIFA's

medical team categorizes the players' age into one of 6 age classes [1] (see figure 1).

Growth plate structure is similar to cartilage, softer and weaker than bone. In the Radius, under normal conditions, 70% of the growth takes place at the distal metaphysis, while 30% occurs in the proximal area. In fact, growth plate is the weakest part of a bone and since its structure is analogous to cartilage, we can see it as a transparent line in radiography images. At the end of adolescent ages, the growth plate turns into bone and would not grow any more. In this case we can say the growth plate is closed [3] [4].

The 3D level set method is recommended to extract the growth plate correctly. The reason of using this 3D approach is accessing the information of adjacent pixels for improving the method's accuracy. Furthermore, the level set method can detect the topologic changes correctly. For a correct execution of this method, an initial contour should be provided, which is derived from the segmented growth plate of previous section [5].

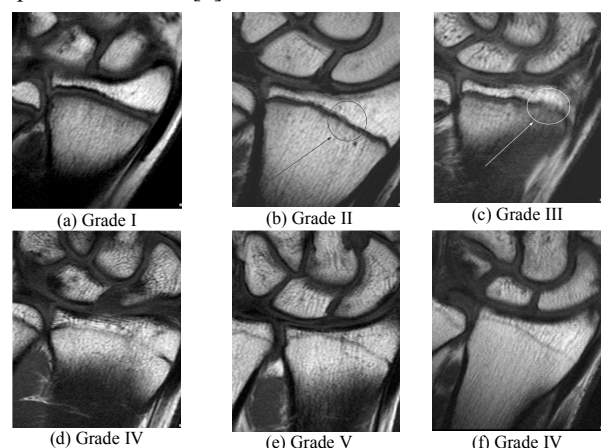


**Fig 1.** The mandatory use of MRI was introduced by FIFA in 2007 as follows: (a) Completely unfused. (b) Early fusion. (c) Trabecular fusion of less than 50% of radial cross-sectional area. (d) Trabecular fusion of more than 50% of radial cross-sectional area. (e) Residual Physis, less than 5 mm on any one section. (f) Completely fused, [1].

## II. METHOD

A framework was designed that requires a set of MR images including the hand wrist information as input, and segmentation of the Growth plate of Radius bone as 3D voxel points as output. The individual components of our framework are outlined as follows:

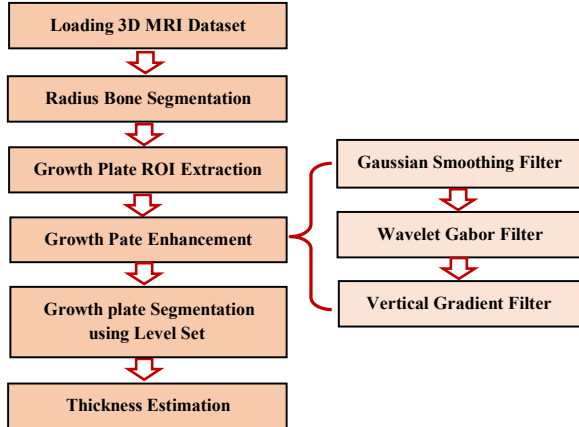


Fig 2. Block diagram of the proposed method.

### A. Radius Bone Segmentation

The next section delves into Radius bone extraction using active contour algorithm. In our previous works [6] [7] a methodological approach based on active contour is proposed for fully automated segmentation of Radius bone. The multi-step approach for segmentation is as following. Since our data set was much noisier, first, as mentioned previously, the noise was eliminated and contrast of the data was enhanced through wavelet transform. The proposed method for MRI image is summarized in Algorithm 1. This algorithm includes the following steps [6]:

**Algorithm 1:** MRI image denoising using wavelets

1. Choosing a type of wavelet ('Biorthogonal wavelets') and the number of levels of decomposition (scales), and computing the DWT (or SWT) of the image to be denoised.
2. Computing an optimal threshold.
3. Selecting shrinkage method and applying the threshold to the wavelet coefficients accordingly.
4. Computing the IDWT (or ISWT) using the thresholded coefficients and determining the denoised image.

Then, an initial segmentation was produced according to the edge map. Next, according to anatomical knowledge about the Radius bone shape and size in intermediate slices, Radius bone was extracted in this slice, and used as the mask slice for adjacent slices.

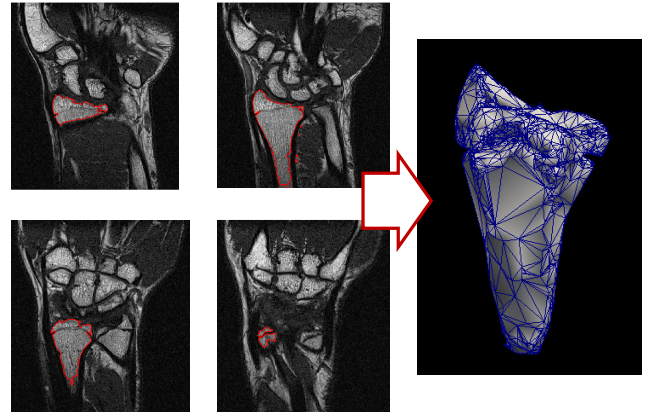


Fig 3. 2D Radius bone segmentation and 3D visualization [7]

This masking procedure was applied to all slices. After that, we derived a convex hull region around the Radius bone. Finally the estimated convex region is used as an initial mask for active contour [6].

### B. ROI Extraction

After extracting the Radius bone, the ROI should be extracted for obtaining the growth plate. As figure 3 illustrates, 3D image of Radius bone is similar to chanterelle ice cream, and its Growth plate is located in the middle and above parts of bone. It approximately seems like a line from coronal view. On the other hand, the bone region of that part is massive, and accordingly has a greater mean than other regions such as bottom long areas of Radius bone; therefore, as figure 5(a) illustrates, intensity of the projected image is higher around growth plate and seems brighter. In the next step, considering the maximum intensity around the growth plate, the explained region can be obtained through deriving the maximum intensity of image and applying a 65% threshold on it. Figure 5(b) shows the convex curve of these regions in yellow color. Figure 5(c) shows the corrected image of figure 5(b) with a horizontal edge for covering the growth plate.

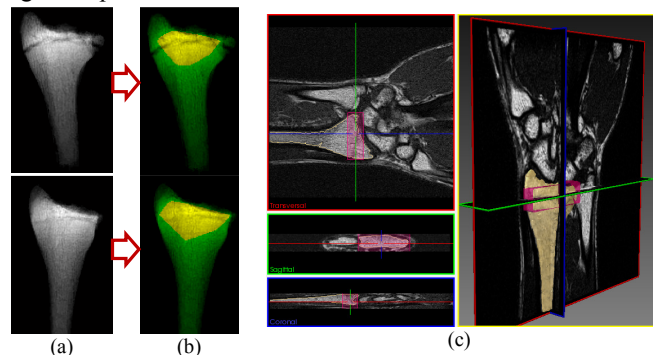


Fig 4. ROI image including growth plate

### C. Growth Plate Enhancement

The growth plates of  $V$  and  $VI$  age classes in wrist MR images are very inconspicuous and difficult to extract (see figure 1(e) and 1(f)). To overcome this problem, some spatial and frequency filters can be used. As figure 6 shows, growth plate has a narrower intensity distribution than its surrounding tissues; so, kernel filters can enhance the closed growth plate contrast effectively. In this section, we propose a two-section algorithm in order to enhance the contrast between growth plate and Radius bone for extracting Physis. Since we want to only enhance the growth plate, typical contrast enhancement techniques are not appropriate. Thus, to increase the homogeneity of same tissues, 3D Gaussian filter is used. Then to better differentiate the growth plate from the bone, Gabor filter and vertical gradient filter in coronal section are used.

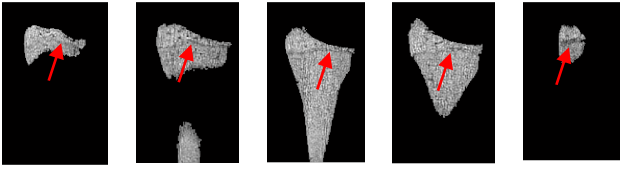


Fig 5. Radius bone and closed Epiphyseal plate inside it in 8, 11,14,17 and 20 coronal slices

### D. Wavelet Gabor Filter

Common contrast enhancement methods are not suitable for solely extracting growth plate due to high amount of Rician noise and partial volume effect, PVE. In MR imaging there is a trade-off between signal-to-noise ratio (SNR), acquisition time and spatial resolution. Another important source of noise in MR images is thermal noise of the human body. Common MR imaging involves sampling in the frequency domain (also called "k-space"), and the MR images are computed using the Inverse Discrete Fourier Transform (IDFT). Signal measurements have components in both real and imaginary channels, and each channel is affected by additive white Gaussian noise. Therefore, the complex reconstructed signal includes a complex white additive Gaussian noise. The PVE is the consequence of the limited resolution of the scanning hardware and discretization procedures. It occurs in non-homogeneous areas, in which several anatomical entities contribute to the gray-level intensity of a single pixel/voxel. It results in blurred intensities across edges, making the task of accurately detecting the borders of two connected objects difficult.

We improve extracting the growth plate through a multi-scale method using Gabor wavelet. Kernel filters are appropriate due to the directed growth plate and their narrow intensity distributions in comparison to surrounding tissues.

**Gaussian filter:** Gaussian filters convolve the image with a Gaussian operator.

$$L_{\sigma}(x, y, \sigma) = N(x, y, \sigma) * I_g(x, y) \quad (1)$$

Where  $I_g$  is grayscale  $I$  and  $*$  is the convolution operator.  $N(x, y, \sigma)$  is an anisotropic Gaussian kernel with zero mean and  $\sigma^2$  variance.

**Gabor Filter:** A Gabor filter is used to enhance the growth plate connection.

$$B(x, y, \lambda, \xi, \theta) = S(x, y, \lambda) \times N(x, y, \zeta, \theta) \quad (2)$$

This filter is defined as the multiplication of a complex sinusoidal and a Gaussian kernel, in which  $S(\cdot)$  and  $N(\cdot)$  are sinusoidal and scaled rotated Gaussian function parts respectively. After convolving the images with a Gaussian filter window, we convolve them with filter bank with different  $\lambda_i$ , scales  $\zeta$ , and orientations  $\theta$ . Then, preserve the maximum response at any point is preserved.

$$G(x, y) = \max_{\lambda, \xi, \theta} (L(x, y) * B(x, y, \lambda, \xi, \theta)) \quad (3)$$

Eq (3) shows the impacts of 3D Gaussian and Gabor filters. Indeed, by using a Gabor wavelet a Gaussian band-pass filter bank with different frequencies and bandwidth in all directions was created, through which the filter's maximum response is derived at any point.

### E. Vertical Gradient Filter

After applying the Gabor wavelet for contrast enhancement, in some heterogeneity regions around the growth plate, due to the sudden change in intensity, oriented Gabor filter connects the growth plate to these regions. We use gradient in perpendicular direction to solve this problem. Another purpose of applying the 3D Gaussian filter, prior to Gabor filter, is reducing this undesirable effect. By applying the vertical gradient, we can enhance the growth plate, which is a thin layer within Radius bone, and attenuate the regions in front of the vertical gradient. This approach partly eliminates the undesirable effect of sudden changes in intensity.

### F. Initialization

As the accurate segmentation is very crucial, we will do the segmentation in different stages. First, an approximate region of growth plate is segmented. Then, the exact segmentation will be achieved using 3D level set algorithm as well as the approximate segmentation of the first stage. Eventually, the growth plate is approximately segmented through anatomical characteristic of axial angle. These stages are elaborated below.

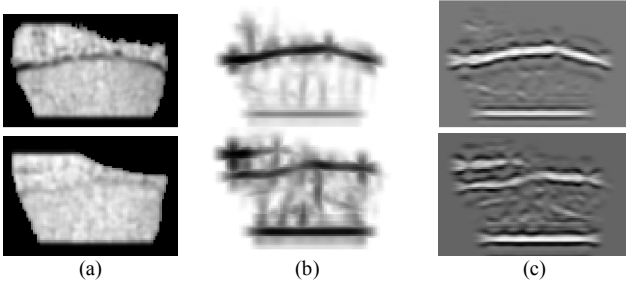


Fig 6. (a) 3D Gaussian filter. (b) Wavelet Gabor filter. (c) Gradient filter

Figure 6 show different steps of the proposed method. Finally, the binary image of each slice is derived through applying the dynamic threshold. Anatomical features of axial slice are employed to extract the growth plate. Axial slices illustrate that the growth plate is located in inner Radius bone, which has a relatively bigger surface. Furthermore, the average intensity is darker than bone tissue due to the Physis existence. Therefore, through using Eq (4), we can calculate the minimum proportion of total intensity to the area in Radius slice, and use it as a mask to select the segmented growth plate.(see figure.7)

$$Epi_{axial} = \min_i \left( \frac{\sum_{all\ pixel} Radius_{axial} \times I_{axial}}{\sum_{all\ pixel} Radius_{axial}} \right) \quad (4)$$

### G. Final Growth Plate Segmentation

Determining the type of window, and also the Radius of initial spheres has a vital role in the quality of segmentation using the local set level method. To further explain the impact of the selected window, one should consider that if the window is selected too small, it will not be able to track the changes in the image [8]. So, the final level sets will be unreal and wrong. On the other hand, if the window is selected too large, the local level set will no longer have a superiority over global ones, and they will be affected by the image heterogeneity. If the window is neither too large nor too small, then image heterogeneity will no longer have an effect on the algorithm [8] [9] [10]. But, the details in the image will be overlooked and segmentation will not be accurate.

$$\frac{\partial \phi}{\partial t} = -(\lambda_1(I - \mu_1)^2 - \lambda_2(I - \mu_2)^2 + \lambda_K + v) \|\nabla \phi\| \quad (5)$$

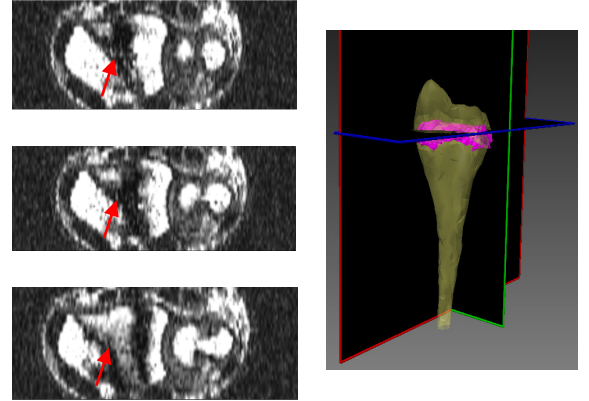


Fig 7. Radius growth plate from different axial slices

Typically, there is no automatic way to choose the size of window, and it is usually selected manually and based on experience. Nevertheless, there are some image indices that make the process of selecting easier and more sensible [11] those parameters are described in the following:

- 1) Considering the resolution of the image can be a good criterion for this purpose. In this research T1-W MRI images with resolution of  $320 \times 280 \times 27$  were used.
- 2) The second point to consider for selecting the appropriate radius is the dimension of the elements existing in the image i.e. what percent of the image is occupied by this element. By considering this fact and image resolution, a proper initial point for finding the right radius can be determined. In this research the radius of 5 pixels was selected using try and false method.

These two coefficients indicate the tendency of the level sets towards the inner or outer parts of the image. In normal situations the two coefficients are set to 1 i.e. the energy inside and outside of the image are equal [12].

Considering the structure of the image and the tendency of level sets towards gathering or departing from the object, one can change these coefficients. The coefficients are changed relatively and the level sets tend to move toward the one with larger value. For example, if in the normal situation the level sets pass the borders of the objects, this can be corrected by increasing the value of  $\lambda_1$ . Another example is when the level sets tend to diverge from the object. In such cases, increasing  $\lambda_2$  will help prevent this divergence. In this research the initial mask is larger than the growth plate; so,  $\lambda_1$  is chosen equal to  $1/8$  and  $\lambda_2$  is set to 1.

### III. EXPERIMENTAL RESULTS

#### A. Data Acquisition

Our data includes 30 sets of MRI T1-weighted images of hand wrist. All images were acquired by Siemens 1.5 Tesla scanner, Magnetom Avanto 18-channel of Payambaran Hospital's imaging center (Abazar St, Tehran, Iran). All subject players aged between 14 -18 and because of exercise and physical training are less exposed to disorders resulted from growth hormone. The images delivered to FIFA's medical team contain 9 coronal slices of hand wrist images.

#### B. Segmentation Results

The proposed segmentation algorithm was tested on more than 1080 coronal T1 MR Slices of 30 subjects. Two coefficients, namely  $\lambda_1$  and  $\lambda_2$  can affect the result of level set segmentation. In this research the initial mask is larger than the growth plate; so,  $\lambda_1$  is set to 1/8 and  $\lambda_2$  is set to 1. Finally using a cubical space including  $10 \times 10 \times 3$  spheres as the primary mask of level-set algorithm, a 3D segmentation of Radius growth plate can be applied. Figure 8 shows the results of applying the local 3D level set method.

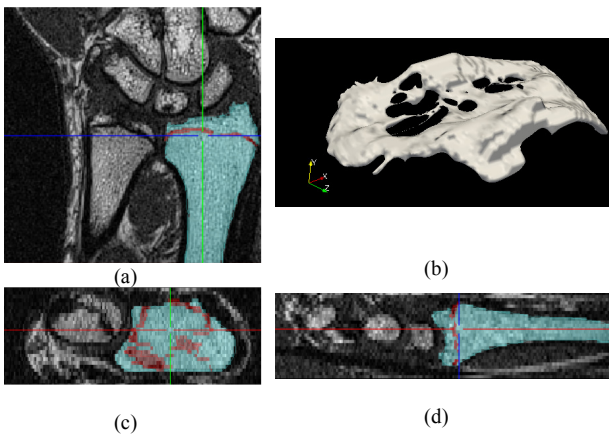


**Fig 8.** Result of local 3D level set segmentation in (a) coronal slice, (b) volumetric of growth plate, (c) axial slice, (d) sagittal slice

In comparison to manual segmentation, our method showed an average Dice similarity coefficient, DSC, and kappa statistics of 89.37% and 86.71% respectively. Unlike other segmentation approaches, the proposed algorithm is fully automatic and does not have the problem of convergence.

**Table 1.** Segmentation quality evaluated using Dice, Sensitivity, Kappa

Dice	Sensitivity	Kappa statistics
89.37% $\pm$ 3.9%	85.80% $\pm$ 5.4%	86.71% $\pm$ 3.1%

#### C. Thickness Estimation

To select the thickness, the ratio of area to circumference is used: the thinner the thickness of growth plate, the older the bone, the smaller the area and the larger the circumference. This criterion is a good factor to separate data sets with different thickness values. On the other hand, this criterion can be evaluated in any data set. In the middle sections, the thickness is smaller than the primary and terminal sections [14]. The following diagram confirms this result for a specific data.

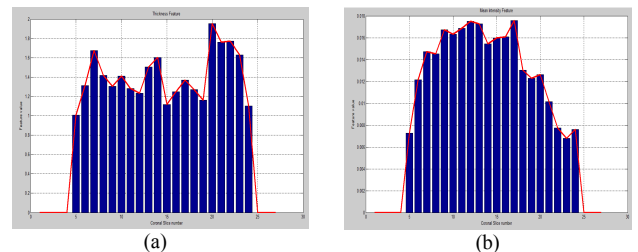


**Fig 9.** (a) Thickness estimation of growth plate (b) Average of intensity in each coronal slice (brighter slices demonstrait ossifying growth plates)

### IV. CONCLUSION

In this study, the Radius growth plate would be fully automatically segmented using level set algorithm. The most challenging part of our work is the accurate segmentation for players whose growth plates have already been closed or is closing as a result of aging. In this situations, ossifying the cartilage like Physis is minimized and the growth plate turns into line. (age orders *V* and *VI* in figure 1 ). On the other hand, different countries' federations are very concerned about the actual age orders. Due to high amounts of rician noise and PVE, segmentation of this part is very difficult.. We applied the algorithm to the MR images of 30 subjects' hand wrists. Our method does not need the human intervention or seed points. Although segmentation techniques are developing rapidly, many recent applications are still based on available manual or semi-manual segmentation tools, for example, MRicro and Amirar. Manually labeling is time consuming and inaccurate even for 2D shapes. Therefore, such a manual approach is impractical for 3D shapes [3]. In the future works we utilize the proposed approach as part of a computer-aided diagnosis system for legal age determination.

## ACKNOWLEDGMENT

We appreciate the radiology authorities of Medical Imaging Informatics Research Center who provided us the data we used in this study.

## REFERENCES

- [1] J.Dvorak, J.George, A.Junge, and J.Hodler "Age determination by magnetic resonance imaging of the wrist in adolescent male football players," *Br J Sports Med.* 2007 Jan; 41(1): 45–52.
- [2] R.Malina, J.C.Eisenmann, S.P.Cumming. et al "Maturity-associated variation in the growth and functional capacities of youth football (soccer) players 13–15 years," *Eur J Appl Physiol* 2004.
- [3] W .Helsen, Van J.Winckel, M.Williams. "The relative age effect in youth soccer accross europe." *J Sports Sci* 2005.
- [4] A. R. Padhani and D.-M. Koh, "Diffusion MR imaging for monitoring of treatment response," *Magnetic resonance imaging clinics of North America*, vol. 19, no. 1, pp. 181–209, Feb. 2011.
- [5] T. Chan and Z. Wei, "Level Set Based Shape Prior Segmentation," in *Computer Vision and Pattern Recognition 2005*, vol. 2, pp. 1164–1170.
- [6] H.Yousefi, M.Fatehi, M.Amian , R.A.Zoroofi " A Fully Automated Segmentation of Radius Bone Based on Active Contour in Wrist MRI Data Set",*20th Iranian Conference on Biomedical Engineering, Tehran, Iran, ICBME 2013.*
- [7] H.Yousefi, M.Fatehi, M.Bahrami R.A.Zoroofi "3D Statistical Shape Models of Radius Bone for Segmentation in Multi Resolution MRI Data Sets", *21th Iranian Conference on Biomedical Engineering, Tehran, Iran, ICBME 2014*
- [8] F. Sanaei Nezhad, A. Fathi Kazerooni, A. Padhani, H. Soltanian Zadeh, and H. Saligheh Rad, "Accurate Monitoring of the Treatment Response in Bone Marrow Metastatic Cancers Based on ADC Histogram Analysis Employing an Automatic Multiparametric (T1/ADC) Bone Marrow Registration/Segmentation Approach," in *ISMRM 2013*.
- [9] T. Chan and L. Vese, "Active contours without edges," *IEEE Trans. Image. Process*, vol. 10, no. 2, pp. 266–277, 2001.
- [10] R. Ronfard, "Region-based strategies for active contour models," *Int. J. Comput. Vis.*, vol. 13, no. 2, pp. 229–251, 1994.
- [11] C. Samson, L. Blanc-Feraud, G. Aubert, and J. Zerubia, "A variational model for image classification and restoration," *IEEE Trans. Pattern Anal. Mach. Intell.*, vol. 22, no. 5, pp. 460–472, 2000.
- [12] N. Verma, S. Member, G. S. Muralidhar, A. C. Bovik, M. C. Cowperthwaite, M. K. Markey, and S. Member, "Model-driven , probabilistic level set based segmentation of magnetic resonance images of the brain," in *EMBC 2011*, pp. 2821–2824.
- [13] S. Lankton and A. Tannenbaum, "Localizing region-based active contours," *IEEE transactions on image processing*, vol. 17, no. 11, pp. 2029–39, Nov. 2008.
- [14] A.F.Roche, Chumlea W C, Thissen D. "Assessment of skeletal maturity of the hand-wrist: Fels method," *Springfield, IL: Charles C Thomas, 1988.*